kCARTA : A fast pseudo line-by-line radiative transfer algorithm with analytic Jacobians, fluxes, Non-Local Thermodynamic Equilibrium and scattering for the infrared

Sergio DeSouza-Machado[1], L. Larrabee Strow[1,2], Howard Motteler[1], and Scott Hannon[3]

[1]JCET, University of Maryland Baltimore County, Baltimore, Maryland
[2]Dept of Physics, University of Maryland Baltimore County, Baltimore, Maryland
[3]Deceased

Correspondence: Sergio DeSouza-Machado (sergio@umbc.edu)

Abstract.

A fast pseudo-monochromatic radiative transfer package using a Singular Value Decomposition (SVD) compressed atmospheric optical depth database has been developed, primarily for simulating radiances from hyperspectral sounding instruments (resolution $\geq$ 0. 1 cm^{-1}). The package has been tested extensively for clear sky radiative transfer cases, using field campaign data and satellite instrument data. The current database uses HITRAN 2016 line parameters and is primed for use in the spectral region spanning 605 cm^{-1} to 2830 cm^{-1}. Optical depths for other spectral regions (15-605 cm^{-1} and 2830-45000 cm^{-1}) can also be generated for use by kCARTA. The clear sky radiative transfer model computes the background thermal radiation quickly and accurately using a layer-varying diffusivity angle at each spectral point; it takes less than 30 seconds (on a 2.8 GHz core using 4 threads) to complete a radiance calculation spanning the infrared. The code can also compute Non Local Thermodynamic Equilibrium effects for the 4 μm CO_2 region, as well as analytic temperature, gas and surface jacobians. The package also includes flux and heating rate calculations, and an interface to a scattering model.

1 Introduction

Recent years have seen the launch and routine operation of new generation infrared sounders on board Earth orbiting satellites, for the purposes of providing measurements for data assimilation into Numerical Weather Prediction (NWP) centers and for monitoring atmospheric composition. These hyperspectral instruments have low noise channels with high resolution ($\geq$ 0.5 cm^{-1}), and provide gigabytes of data daily, from about 620 - 2800 cm^{-1}. Examples include the Atmospheric InfraRed Sounder (AIRS)(Aumann et al., 2003) on board NASA's Aqua satellite, the Infrared Atmospheric Sounding Interferometer (IASI) on board the Metop satellites (Clerbaux et al., 2009) and the Cross Track Infrared Sounder (CrIS) on board the Suomi and JPSS-1 satellites (Han et al., 2013).

The radiances measured by these instruments are obtained under all-sky conditions (*i.e.* clear or cloudy). Publicly available thermodynamic profiles retrieved from this voluminous data are presently performed *after* cloud-clearing the radiances (Susskind et al., 1998). Monochromatic line-by-line (MNLBL) codes are too slow for use in the operational retrievals from

the cloud-cleared radiances. Instead, optical depths (or transmittances) produced by these MNLBL codes are parametrized for use in fast Radiative Transfer Algorithms (RTAs), at the instrument resolution. The accuracy of the retrieved products depends on the accuracy of the fast models, which underlines the importance of the accuracy of line parameters and lineshapes used in MNLBL codes, particularly the far-wing effects.

To satisfy the accuracy requirements of convolved optical depths and radiances used in developing and testing these fast models, the high altitude (doppler broadened) lines need to have monochromatic spectral resolutions of 0.0025 cm^{-1} or better over the almost 2500 cm^{-1} span of a typical infrared sounder. Using true MNLBL codes to produce optical depths for training the fast models is computationally intensive, as accurate lineshapes needed to be computed for millions of spectral points, each at about 100 layers spanning a 0-80 km atmosphere, for about 40-50 gases; this has to be done for 50 or more profiles. The acceleration of this part of the process, needed to develop a fast RTA for the AIRS sounder, was the motivating factor behind the development of the work presented here. For this we also developed a line-by-line code (referred to as UMBC-LBL) to produce an accurate pre-computed database of monochromatic atmospheric optical depths. Singular Value Decomposition (SVD) was then used to produce a highly compressed database (referred to as the kCompressed database (Strow et al., 1998)) that is highly accurate, relatively small, and easy to use. When coupled to an accurate radiative transfer code, this pseudo line-by-line package can be used as a starting point for developing tools for atmospheric retrievals (Rodgers, 2000). The key point to note is that though some optical depth information may be lost due to the compression and/or resolution of the database, *the convolved radiances* are very accurate.

To compute optical depths and radiances at any level for an arbitrary Earth atmospheric thermodynamic + gas profile, we paired together an uncompression algorithm for the kCompressed database with a one dimensional clear sky radiative transfer algorithm (RTA). The RTA works for both a downlooking and an uplooking instrument, with geometric ray tracing accounting for the spherical atmospheric layers. The generation of monochromatic transmittances from the compressed database is at least an order of magnitude faster than using a MNLBL code; for the long paths in the atmosphere the computed transmittances are smooth and well behaved, and can be used to develop fast forward models. Radiances computed using the compressed database are as accurate as those computed with a MNLBL code as our compression procedure introduces errors well below spectroscopy errors (Strow et al., 1998).

The entire package is called kCARTA, which stands for "kCompressed Atmospheric Radiative Transfer Algorithm". Although kCARTA *is* much slower than fast forward models which use effective convolved transmittances, it is much more accurate, and can be used to generate optical depths and transmittances for developing the faster models. An example is the Stand Alone Radiative Transfer Algorithm (SARTA) (Strow et al., 2003) for which kCARTA is the Reference Forward Model; SARTA is used to retrieve Level 2 geophysical products from the AIRS (Strow et al., 2003) and CriS (Gambacorta, 2013) instruments. Other fast forward models for the infrared which parametrize the transmittances of the finite width instrument channels include a Principal Component based Radiative Transfer Model (PCRTM; (Liu et al., 2006)), Radiative Transfer for TIROS Operational Vertical Sounder (RTTOV; (Saunders et al., 1999)) and the Jülich Rapid Spectral Simulation Code (JURASSIC; (Hoffman and Alexander, 2009)).

kCARTA also includes algorithms to rapidly compute analytic jacobians, and is available in a Fortran 90 package. This package (v1.21, April 2019) uses some of the newer Fortran features such as implicit loops, function overloading and modules, and includes code for computing fluxes, heating rates, and the effects of cloud and aerosol scattering using the Parametrization of Clouds for Longwave Scattering in Atmospheric Models (PCLSAM) (Chou et al., 1999) algorithm. While kCARTA was developed for use in the infrared region (605-2830 cm^{-1}), it is trivial to extend the database out in either direction, to span the Far InfraRed to the Ultra-Violet. A clear-sky only radiance+jacobian Matlab version is also available.

The speed and accuracy, plus available run-time options of the code make it a very attractive alternative to other existing line by line codes. The literature is replete with papers and books describing spectroscopic calculations, monochromatic radiative transfer and flux calculations (see for example (Goody and Yung, 1989; Edwards, 1992; Clough et al., 1992; Clough and Iacono, 1995; Tjemkes et al., 2002; Buehler et al., 2011; Schreier et al., 2014; Dudhia, 2017; Vincent and Dudhia, 2017)) so here we chose to emphasize the features (and limitations) of kCARTA that would interest researchers working in these and related fields, and apply kCARTA to quantify how different spectroscopic databases impact simulated clear-sky Top of Atmosphere (TOA) brightness temperatures. Focusing on the infrared (605 - 2830 cm^{-1}) region, this paper begins with a description of the line-by-line code and the kCompressed database, followed by a description of the clear sky radiative transfer algorithm, together with jacobians. The paper then discusses in detail some of the internal machinery of kCARTA, such as a background thermal computation developed for kCARTA, flux computations and scattering packages.

2 Overview of line-by-line code and kCompressed Database

2.1 UMBC-LBL

For an input set of [average temperature, pressure and gas amount (in molecules/cm^2)] parameters, a custom monochromatic line-by-line code (UMBC-LBL) (De Souza-Machado et al., 2002) has been developed in order to accurately compute optical depths. This code defaults to the Van Vleck and Huber lineshape (Van Vleck and Huber, 1977; Clough et al., 1980) for almost all molecules, using spectroscopic line parameters from the HIgh-resolution TRANsmission (HITRAN) molecular absorption database.

For each spectral region the UMBC-LBL optical depth computations are divided into bins that are typically 1 cm^{-1} wide in the infrared. The optical depth in each of these bins is accumulated in three stages as shown in Figure 1 : (1) fine mesh stage - absorption due to line centers within 1 cm^{-1} of the bin edges is included at a very high resolution (typically 0.0005 cm^{-1}) and then five point boxcar integrated to the output (typically 0.0025 cm^{-1}) grid; in Figure 1 these are the red lines within the bin edges at $\pm$ 0.5 cm^{-1} and the blue lines within 1 cm^{-1} of the same bin edges (2) medium mesh stage - absorption from line centers within 1-2 cm^{-1} of the bin edges is included at 0.1 cm^{-1} resolution, shown in green in the figure and finally (3) coarse mesh stage - absorption from line centers within 2-25 cm^{-1} of the bin edges, are included at 0.5 cm^{-1} resolution (none shown in the figure); for (2) and (3) the results are interpolated to the output grid. The black line is the accumulated optical depth for that bin.

We note three points here. First, the default kCARTA uses 0.0005 cm^{-1} resolution between 605-880 cm^{-1} and 0.0025 cm^{-1} from 805-2830 cm^{-1} (after the 5 point boxcar). Section 7 demonstrates convolved radiances computed with these resolutions compare very well against other RTAs, especially after convolving with a typical hyperspectral sounder response function. Second, the above line-by-line computations are very similar to those in other models (Edwards, 1992; Dudhia, 2017), but we use the "medium" bins and "coarse" bins for the lines whose centers are within the intervals lying $\pm$ [1,2] and $\pm$ [2,25] cm-1 respectively of the bin edges, instead of using only "coarse" bins. Thirdly we note that for most Earth atmosphere molecules, the line strength $\times$ gas amount combination means the optical depth contribution due to line centers further than 25 cm^{-1} away from the bin is negligible and can be ignored (Dudhia, 2017); the exception for the Earth atmosphere are H_2O and CO_2 which have countless strong lines further than 25 cm^{-1} away from bin edges. To speed up the optical depth calculations, the weak but non-negligible contribution from these "far lines" is added in using a continuum optical depth contribution which depends on temperature and gas absorber amount.

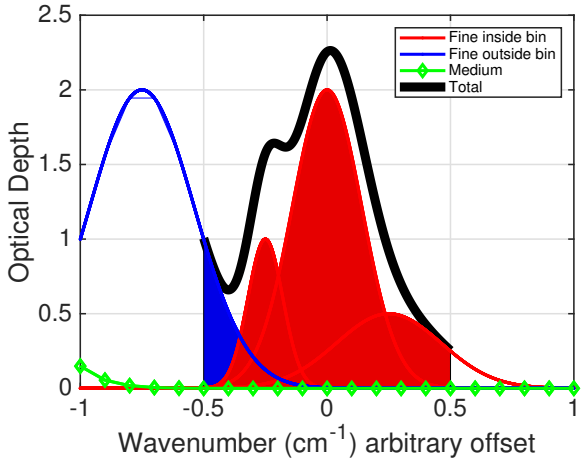

Figure 1. Line-by-line calculations from UMBC-LBL. The bin of interest is at (-0.5,+0.5) cm^{-1}. Lineshapes whose line centers are within this bin (red) and within $\pm$ 1cm^{-1} of the bin edge (blue) are computed using high spectral resolution; line centers that are further out (green) have the lineshapes computed at medium resolution and then interpolated to a higher resolution; line centers even further away (not shown) are computed at coarse resolution. The black curve is the sum over all the line contributions within that bin.

The above steps are followed for almost all molecules. Modifications to the above steps are needed for water vapor (which is separated into the traditional "basement" plus "continuum" contributions (Clough et al., 1980, 1989)) and CO_2 in the 4 and 15 μm region which needs line-mixing lineshapes (Strow and Pine, 1988; Tobin et al., 1996; Niro et al., 2005; Lamouroux et al., 2015). Other molecules have optical depths that are more easily modeled with the Van Huber lineshape, though recently the infrared absorption due to CH_4 has been modeled using line mixing (Tran et al., 2006). The UMBC-LBL optical depth computation for water vapor should be robust at all frequencies, and allows the addition of water continuum models such as the recent MT-CKD 3.2 coefficients (Mlawer et al., 2012). Spectra from UMBC-LBL have been extensively compared against

optical depths computed by models such as Line-by-line Radiative Transfer Model (LBLRTM) (Clough et al., 1992, 2005) and the General line-by-line Atmospheric Transmittance and Radiance model (GENLN2) (Edwards, 1992).

2.2 kCompressed database

When applied toward any realistic Earth atmosphere simulation for an observing instrument, the UMBC-LBL calculations described above become impractically slow as they need to be performed for multiple gases in the atmosphere, over ~ 100 atmospheric layers and encompassing a wide spectral range.

UMBC-LBL is therefore primarily used to generate an uncompressed database of look-up tables as described below. For each gas other than water vapor, the spectra are computed using the US Standard Atmosphere temperature profile, as well as five temperature offsets (in steps of 10K) on either side of the temperature profile, for a total of 11 temperatures. Tests using NWP profiles show this is usually sufficient everywhere except for a handful over the winter Antartica, which could fall slightly outside the coldest offset (on average by about 3 K) between 600-1000 mb; kCARTA handles these extreme cold cases by extrapolating what has been compressed and zero checking the optical depths.

The default infrared database spans 605-880 cm^{-1} and 805-2830 cm^{-1}, broken up into 10000 point intervals that are 5 cm^{-1} and 25 cm^{-1} wide respectively. Each file contains matrices to compute optical depths for these 10000 points at the set resolution. The one hundred average pressure layers used in making the database are from the AIRS Fast Forward Model. The layers span 1100 mb to 0.005 mb (about ground level to 85 km), and were chosen such that there is less that 0.1 K Brightness Temperature (BT) errors in the simulated AIRS radiances. The layers are about 200 m thick at the bottom of the atmosphere, gradually getting thicker with height (about 0.65 km at 10 km and 6 km at an altitude of 80 km).

These $10000 \times 100 \times 11$ optical depths intervals are then compressed using Singular Value Decomposition (SVD) to produce the kCompressed Database. Each compressed file will have a matrix of basis vectors B (size $10000 \times N$), and compressed optical depths D' (size $N \times 100 \times 11$), where N is the number of significant singular vectors found. The prime denotes the compression worked more efficiently when the optical depths were scaled to the (1/4) power (Strow et al., 1998; Rodgers, 2000).

The self broadening of water is accounted for by generating monochromatic lookup tables for the reference water amount, multiplied by 0.1, 1.0, 3.3, 6.7 and 10.0 at the eleven temperature profiles specified above, meaning D' for water will have an extra dimension of length 5. Note that for the infrared we treat the HDO isotope (HITRAN isotope 4) as a separate gas from the rest of the water vapor isotopes.

The compressed optical depths D' vary smoothly in pressure, meaning the user is not limited to only using the 100 AIRS layers. For an arbitrary pressure layering, the look-up tables are uncompressed using spline or linear interpolation in temperature and pressure, and scaled in gas absorber amount. Temperature interpolation of matrix D' for an AIRS 100 layer atmosphere therefore results in a matrix D'' of size $N \times 100$, and the final optical depths (of size 10000×100) are computed using $(BD'')^4$. Both the spline and linear interpolations allow easy computation of the analytic temperature derivatives, from which kCARTA can rapidly compute analytic jacobians (see Section 5). The cumulative optical depth for each layer in the atmosphere is obtained by a weighted sum of the individual gas optical depths, with accuracy limited by that of the compressed database (Strow

et al., 1998). The interested reader is referred to (Vincent and Dudhia, 2017) for a further discussion of other RTAs that use compressed databases.

The most recent kCompressed database uses line parameters from the HITRAN 2016 database (Rothman et al., 2013; Gordon et al., 2017), which together with the UMBC-LBL lineshape models, determine the accuracy of the spectral optical depths in this database. UMBC-LBL CO_2 line-mixing calculations use parameters that were derived a few years ago. Newer line-mixing models exist and we now use optical depths computed using LBLRTM v12.8 together with the line parameter database file based on HITRAN 2012 (aer_v_3.6), and (a) CO_2 line mixing by (Lamouroux et al., 2010, 2015)) and (b) CH_4 line mixing by (Tran et al., 2006).

In addition complete kCompressed databases for the IR using optical depths only from HITRAN 2012, LBLRTM v12.4 code and from GEISA 2015 (Husson et al., 2015) have been generated for comparison purposes. At compile time we usually point kCARTA to the HITRAN 2016 kCompressed database made by UMBC-LBL, but at run time we have switches that easily allow us to swap in for example the CO_2 and CH_4 tables generated from LBLRTM.

The original lookup tables for the thermal infrared occupy hundreds of gigabytes, while the compressed monochromatic absorption coefficients are a much more manageable 824 megabytes (218 megabytes (water+HDO) + 76 megabytes (CO2) + 530 megabytes (about 40 other molecular and 30 cross section gases)). A general overview of some of the factors involved in compressing look-up tables for use in speeding up line-by-line codes is found in (Vincent and Dudhia, 2017), while more details about the detailed testing and generation of the kCARTA SVD compressed database are found in (Strow et al., 1998). Appendix B discusses the extension of the database to span 15 cm^{-1} to 44000 cm^{-1}, though we note that kCARTA lacks built-in accurate scattering calculations in the shorter wavelengths. In order to resolve the narrow doppler lines at the top-of-atmosphere, the resolution $\delta\nu$ of the spectral bands in Appendix B is adjusted according to $\delta\nu \sim \nu_0\sqrt{(k_bT/m)}/c$, where ν_0 is the band center, and T, m are the temperature and mass of the molecule respectively, while k_b and c are Boltzmann's constant and speed of light.

The default kCARTA mode is to use the first 42 molecular gases in the HITRAN database, together with about 30 cross-section gases, for which we have reference profiles. If the user does not provide the profiles for any of these gases, kCARTA uses the US Standard profile for that gas. The user can also choose to only use a selected number of specified gases. While running kCARTA, the user can then define different sets of mixed paths, where some of the gases are either turned off or the entire profile is multiplied by a constant number, which is very useful when for example we want to include only certain gases when we parametrize optical depths for SARTA.

3 kCARTA Clear sky radiative transfer algorithm

As a stream of radiation propagates through a layer, the change in diffuse beam intensity $R(\nu)$ in a plane parallel medium is given by the standard Schwarschild equation (Liou, 1980; Goody and Yung, 1989; Edwards, 1992)

$$\mu\frac{dR(\nu)}{dk_e} = -R(\nu) + J(\nu) \tag{1}$$

where μ is the cosine of the viewing angle, k_e is the extinction optical depth, ν is the wavenumber and $J(\nu)$ is the source function. For a non-scattering "clear sky", the source function is usually the Planck emission $B(\nu,T)$ at the layer temperature T, leading to an equation that can easily be solved for an individual layer. The general solution for a downlooking instrument measuring radiation propagating up through a clear-sky atmosphere can be written in terms of four components :

$$R(\nu) = R_{\rm s}(\nu) + R_{\rm lay}(\nu) + R_{\rm th}(\nu) + R_{\rm solar}(\nu) \tag{2}$$

which are the surface, layer emissions, downward thermal and solar terms respectively. In terms of integrals the expressions can be written as (see e.g. (Liou, 1980; Dudhia, 2017))

$$\begin{aligned} R(\nu,\theta) = \epsilon_s(\nu) B(\nu,T_s) \tau_{atm}(\nu,\theta) + \int_{surface}^{TOA} B(\nu,T(z)) \frac{\partial \tau(\nu,\theta)}{\partial s} ds + \\ \frac{1-\epsilon_s(\nu)}{\pi} \tau_{atm}(\nu) \int d\Omega^+ \int_{TOA}^{surface} B(\nu,T(s)) \frac{\partial \tau(\Omega)}{\partial s} cos(\theta) ds + \\ \rho_s(\nu) B_{\odot}(\nu) cos(\theta_{\odot}) \tau_{atm}(\nu,\theta_{\odot}) \tau_{atm}(\nu,\theta) \end{aligned} \tag{3}$$

where $B(\nu,T)$ is the Planck radiance at temperature T, T_s is the skin surface temperature, ϵ_s, ρ_s are the surface emissivity and reflectivity; $B_{\odot}(\nu)$ is the solar radiance at TOA, $\theta_{\odot}$ is the solar zenith angle; θ is the satellite viewing angle, $\tau(\nu,\theta)$ is the transmission at angle θ while τ_{atm} is the total atmospheric transmission. The $d\Omega^+$ in the middle term indicates integration over the upper hemisphere.

In what follows we discretize Eqn. 2 so that layer $i = 1$ is the bottom and $i = N$ (=100) the uppermost, schematically shown in Figure 2 for a clear sky four layer atmosphere, with *O* being the center of the Earth. *A* is the satellite while *S* is the satellite sub-point directly below it. Point *P* is the ground scene being observed by the satellite (slightly away from nadir), and *N* is the local normal at *P*. ∠SAP is the satellite scan angle while ∠APN is the satellite zenith angle θ; ∠NPI is the solar zenith angle $\theta_{\odot}$. Note that as the radiation propagates through the pressure layers from *P* to H_1 to H_2 to H_3 to H_4 to *A*, the local angle (between the radiation ray and the local normal at any of the concentric circles) keeps changing due to the spherical geometry of the layers (refraction effects can also be included).

The default mode of kCARTA (f90) assumes linear variation of layer temperature with optical depth, uses a background thermal diffusive angle that varies with the layer-to-ground optical depth (instead of a constant value typically assumed to be $cos^{-1}(3/5)$) and does ray-tracing to account for the spherical atmospheric layers (but with no density effects). The f90 version of kCARTA also allows the user to choose constant layer temperature, and to choose alternate ways of computing the background term, which will be discussed in Section 6.

Here we describe radiative transfer for the constant layer temperature case; see Section 6.2 for a short discussion when using the linear-in-tau option. For an arbitrary layer i with (nadir) optical depth $k_i(\nu)$, the transmittance of a beam passing from the

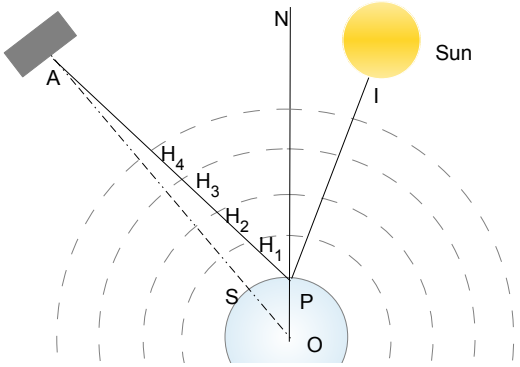

Figure 2. Viewing geometry for the sounders modeled by kCARTA. *A* is the satellite and point *P* is being observed by the satellite, while *I* is the sun

bottom to the top of the layer at angle θ is given by $\tau_i(\nu,\theta) = e^{-k_i(\nu)/cos(\theta)}$. The transmittance from the top of layer i to space is then the product of the individual transmittances of the layers above i

$$\tau_{i+1\rightarrow TOA}(\nu,\theta) = \pi_{j=i+1}^{N}\tau_j(\nu,\theta) \tag{4}$$

with the special case of transmission from ground to space $(i = 0)$ involving all N layers.

The individual contributions to the upwelling radiance are then computed as follows.

3.1 Surface emission

The kCARTA surface emission is given by

$$R_s(\nu) \quad = \quad \epsilon_s(\nu)B(\nu,T_s)\tau_{GND\rightarrow TOA}(\nu,\theta) \tag{5}$$

where $\epsilon_s(nu)$ is the user supplied emissivity.

3.2 Layer emission

The atmospheric absorption and re-emission is modeled as :

$$R_{\text{lay}} \quad = \quad \sum_{i=1}^{i=N} B(\nu,T_i)(1.0-\tau_i(\nu))\tau_{i+1\rightarrow TOA}(\nu,\theta) \tag{6}$$

Layers with negligible absorption ($\tau_i \rightarrow 1$) contribute negligibly to the overall radiance, while those with large optical depths ($\tau_i \rightarrow 0$) "black" out radiation from below. $(1.0-\tau_i(\nu))$ is the emissivity of the layer while $(1.0-\tau_i(\nu))\tau_{i+1\rightarrow TOA}(\nu,\theta)$ is the weighting function W_i of the layer.

3.3 Background thermal radiation

The atmosphere also emits radiation downward, *at all angles*, in a manner analogous to the upward layer emission just discussed. The total background thermal radiance at the surface is an integral over all (zenith and azimuth) radiance streams propagating from the top-of-atmosphere (set to 2.7 K) to surface. This is time consuming to compute using quadrature, and one approximation is to use a single effective (or diffusivity) angle of $\theta_{diff} = cos^{-1}(3/5)$ at all layers and wavenumbers :

$$R_{th}^{surface}(\nu) = \pi\rho_s \sum_{i=N}^{i=1} B(T_i)\left[\tau_{i-1\rightarrow ground}(\nu,\theta_{diff}) - \tau_{i\rightarrow ground}(\nu,\theta_{diff})\right] \quad (7)$$

The summation is from top-of-atmosphere to ground, and ρ_s is the surface reflectivity discussed above. Current sounders have channel radiance accuracy better than 0.2K, so while the above term is much smaller than the surface or upwelling atmospheric emission contributions, it has to be computed accurately. Section 6 includes a detailed discussion of how kCARTA improves the accuracy of this background term by using a look-up table to rapidly compute a spectrally and layer varying diffusive angle.

3.4 Solar radiation

Letting the surface reflectivity be denoted by $\rho_s(\nu,\theta,\phi)$, then the solar contribution to the TOA radiance is given by

$$R_{\odot}(\nu) = \rho_s(\nu,\theta,\phi)B_{\odot}(\nu)cos(\theta_{\odot}) \times \tau_{N\rightarrow ground}(\nu,\theta_{\odot}))\tau_{ground\rightarrow TOA}(\nu,\theta))\Omega_{\odot} \quad (8)$$

where $B_{\odot}(\nu)$ is the solar radiation at the top of atmosphere and accounts for the solar disk. Over ocean, if the wind speed and solar and satellite azimuth angles are known, the reflectivity can be pre-computed using the Bi-directional Reflectance Distribution Function (BRDF) and input to kCARTA; see for example Appendix C in (Nalli et al., 2016). It is not easy to compute the BRDF over land, and the reflectivity could be simply modeled as $\rho_s(\nu) = \frac{1-\epsilon_s(\nu)}{\pi}$.

$\Omega_{\odot} = \pi(r_s/d_{se})^2$ is the solid angle subtended at the earth by the sun, where r_e is the radius of the sun and d_{se} is the earth-sun distance. The solar radiation incident at the TOA $B_{\odot}(\nu)$ comes from data files related to the ATMOS mission (Farmer et al., 1987; Farmer and Norton, 1989), and is modulated by the angle the sun makes with the vertical, $cos(\theta_{\odot})$ (day-of-year effects are not included in the earth-sun distance).

4 Non Local Thermodynamic Equilibrium computations

During the daytime, incident solar radiation is preferentially absorbed by some CO_2 and O_3 infrared bands, whose kinetic temperature then differs from the rest of the bands or molecules. This leads to enhanced emission by the lines in these bands.

Limb sounders detect NLTE effects in the 15 μm CO_2 bands (and in other molecular bands for example O_3) due to the extremely long paths involved, but these are not modeled in the package as kCARTA is designed for nadir sounders.

For a nadir sounder, the most important effects are seen in the CO_2 4 μm (ν_3) band. kCARTA includes a computationally intensive line-by-line Non Local Thermodynamic Equilibrium (NLTE) model to calculate the effects for this CO_2 band. The model requires the kinetic temperature profile and NLTE vibrational temperatures of the strong bands in this region, to compute the optical depths and Planck modifiers for the strong NLTE bands and the weaker LTE bands (Edwards et al., 1993, 1998; Lopez-Puertas and Taylor, 2001; Zorn et al., 2002), which are then used to compute a monochromatic top-of-atmosphere nadir radiance.

AIRS provided the first high resolution nadir data of NLTE in the 4 micron CO_2 band. Using the kCARTA NLTE line-by-line model, a Fast NLTE Model (De Souza-Machado et al., 2007) for sounders has already been developed, which is used in the NASA AIRS L2 operational product.

5 Clear Sky Jacobian algorithm

Retrievals of atmospheric profiles (temperature, humidity and trace gases) minimize the differences between observations and calculations, by adjusting the profiles using the linear derivatives (or jacobians) of the radiance with respect to the atmospheric parameters. This section describes the computation of analytic jacobians by kCARTA. Note that kCARTA currently computes jacobians and weighting functions using a constant layer temperature assumption. For a downward looking instrument, for simplicity consider only the upwelling terms in the radiance equation (atmospheric layer emission and the surface terms). Assuming a nadir satellite viewing angle, the solution to Equation 1 is :

$$R(\nu) = \epsilon_s B(T_s,\nu)\tau_{1\rightarrow TOA}(\nu) + \Sigma_{i=1}^{i=N} B(T_i,\nu)(1.0-\tau_i(\nu))\tau_{i+1\rightarrow TOA}(\nu) \tag{9}$$

Differentiation with respect to the m-layer variable s_m, (gas amount or layer temperature $s_m = q_{m(g)}, T_m$) yields

$$\frac{\partial R(\nu)}{\partial s_m} = \epsilon_s B(T_s)\frac{\partial \tau_{1\rightarrow TOA}(\nu)}{\partial s_m} + \sum_{i=1}^{N} B(T_i,\nu)(1.0-\tau_i(\nu))\frac{\partial \tau_{i+1}(\nu)}{\partial s_m} + \sum_{i=1}^{N}\tau_{i+1\rightarrow TOA}(\nu)\frac{\partial}{\partial s_m}\left[B(T_i,\nu)(1.0-\tau_i(\nu))\right] \tag{10}$$

where as usual, $\tau_m(\nu) = e^{-k_m(\nu)}$, $\tau_{m\rightarrow TOA}(\nu) = \Pi_{j=m}^{N} e^{-k_j(\nu)}$. The differentiation yields

$$\begin{aligned}\frac{\partial R(\nu)}{\partial s_m} &= \left[\epsilon_s B(T_s)\tau_{1\rightarrow TOA}\right](-1)\frac{\partial k_m(\nu)}{\partial s_m} + \\ &\left[\sum_{i=1}^{m-1}(1.0-\tau_i(\nu))B_i(\nu)\tau(\nu)_{i+1\rightarrow TOA}\right](-1)\frac{\partial k_m(\nu)}{\partial s_m} + \\ &\left[(1.0-\tau_m(\nu))\frac{\partial B_m(\nu)}{\partial s_m} - B(T_m,\nu)\frac{\partial \tau_m(\nu)}{\partial s_m}\right]\tau_{m+1\rightarrow TOA}(\nu)\end{aligned} \tag{11}$$

The individual jacobian terms $\frac{\partial k_m}{\partial s_{m(g)}}$ are rapidly computed by kCARTA, as follows. The gas amount derivative is simply $\frac{\partial k_m}{\partial q_{m(g)}} = \frac{k_m}{q_{m(g)}}$ (with added complexity for water, to account for self broadening), and the temperature derivative $\frac{\partial k_m}{\partial T}$ is cumulatively obtained $while$ kCARTA is performing the temperature interpolations during the individual gas database uncompression.

The solar and background thermal contributions are also included in the jacobian calculations. The thermal background jacobians are computed at $\cos^{-1}(3/5)$ at all levels, for speed. This would lead to slight differences when comparing the jacobians computed as above to those obtained using finite differences. kCARTA also computes the weighting functions, and jacobians with respect to the surface temperature and surface emissivity.

6 Background thermal and temperature variation in a layer

In this section we take a closer look at the computation of downwelling background thermal radiation, and layer temperature variation.

6.1 Background thermal radiation

The contribution of downwelling background thermal to top-of-atmosphere upwelling radiances is negligible in regions that are blacked out as the instrument cannot see surface leaving emission. Similarly in layers/spectral regions where there is very little absorption and re-emission, the contribution is negligible as the effective layer emissivity (denoted by $\Delta\tau_i(\nu)$ below) goes to zero. The background contribution thus needs to be done most accurately in the window regions (low but finite optical depths) ; depending on the surface emissivity (and hence reflectivity) in the window regions, in terms of BT this term contributes as much as 4 K of the total radiance when reflected back up to the top of the atmosphere.

The contribution at the surface by a downwelling radiance stream propagating at angle (θ,ϕ) through layer i is given by

$$\begin{aligned}\Delta R_i(\nu,\theta,\phi) &= B(\nu,T_i)(1.0-\tau_i(\nu,\theta,\phi))\tau_{i-1\rightarrow ground}(\nu,\theta,\phi) \\ &= B(\nu,T_i)(\tau_{i-1\rightarrow ground}(\nu,\theta,\phi)-\tau_{i\rightarrow ground}(\nu,\theta,\phi)) \end{aligned} \quad (12)$$

where θ is the zenith and ϕ is the azimuth angle, and $\tau_{i\rightarrow ground}$ are the layer-to-ground transmittances, derived from layer-to-ground optical depths x. This equation can be rewritten as

$$\Delta R_i(\nu,\theta,\phi) = B(\nu,T_i)\times\Delta\tau_i(\nu,\theta,\phi) \quad (13)$$

An integral over (θ,ϕ) would give the contribution from the layer. The total downwelling spectral radiance at the surface would be a sum over all i layers (and the downwelling flux at the surface would be the integral over all wavenumbers).

The integral over the azimuth is straightforward (assuming isotropic radiation), but the integral over the zenith is more complex. Since the reflected background term is much smaller than the surface or atmospheric terms, a single stream at the effective angle $\theta_{diff} = cos^{-1}(3/5)$ (Liou, 1980) is often used as an approximation, at all layers and wavenumbers.

We have refined the computation as follows. Recall that $\Delta R(\nu)$ in Equation 13 depends on the layer-to-ground optical depth x. Letting $\mu = cos\theta$ the integral over the zenith ($\int_0^1 e^{-x/\mu}\mu d\mu = E_3(x)$, more commonly known as the exponential Integral of

the third kind). The area under the $E_3(x)$ curve would be the total flux coming from all optical depths ($0 \leq x \leq \infty$); over 77% of this area comes from the range $0 \leq x \leq 1$.

Applying the Mean Value Theorem for Integrals (MVTI) to $E_3(x)$, we can write Eq. 13 in terms of two effective diffusive angles $\theta_d^i, \theta_d^{i-1}$ at each layer i :

$$\Delta\tau(i,i-1) = \tau(i-1 \rightarrow ground, \theta_d^{i-1}, \nu) - \tau(i \rightarrow ground, \theta_d^i, \nu)$$
$$R_{th}^{surface}(\nu) = 2\pi\rho_s \sum_{i=N}^{i=1} B(\nu, T_i)\Delta\tau(i,i-1) \tag{14}$$

with the effective angles varying as a function of the layer to ground space optical depth of that layer, and the layer immediately below it. Numerical solutions to the MVTI show that when $x \rightarrow 0$ then $\mu_d \rightarrow 0.5$ (or $\theta_d \rightarrow 60^\circ$). Similarly as $x \rightarrow \infty$ then $\theta_d \rightarrow 0^\circ$, but this optically thick atmosphere means an instrument observing from the TOA cannot see the surface, so we use a lower limit (of 30°) for the diffusive angle. Finally when x = 1.00 we find the special case $\mu_d = 0.59274 \simeq (3/5)$. For "optically thin" regions, the layers closest to the ground contribute most to $R_{th}(\nu)$.

With today's high speed computers, kCARTA uses an effective diffusive angle θ_d tabulated as a function of layer to ground optical depth x, as follows. For each 25 cm^{-1} interval spanning the infrared the layer L above which $cos^{-1}(3/5)$ can be safely used was determined; below this layer, the lookup table is used. The table has higher resolution for $x \leq 0.1$ and becomes more coarse as x increases, with the effective diffusive angle cutoff at 30°when the optical depths are larger than about 15.

We have tested this method of computing the background thermal against both 20 point Gauss-Legendre quadrature and the 3 point exponential Gauss-quadrature (used by LBLRTM flux computations), and found the method to very accurate and fast, both in terms of the downwelling flux at the surface, and also the final TOA computed radiance, even when the emissivity is as low as 0.8 (which means a significant contribution from the reflected thermal). At this low emissivity value, the constant $cos^{-1}(3/5)$ diffusivity angle model produces final TOA BT which differ from the Gauss-Legendre model by as much as 1.3 K (for the tropical profile) at for example 900 cm^{-1}, while the exponential quadrature and our model have errors smaller than 0.005 K.

6.2 Variation of layer temperature with optical depth

LBLRTM (Clough et al., 1992, 2005) has been extensively tested and shown to be very accurate, in its computation of optical depths, radiances and fluxes. In the computation of radiances, both kCARTA and LBLRTM codes use a "linear in τ" layer temperature variation; the former uses a higher order expansion (accurate to $O(\tau^5)$ for small τ), and also has an option to use "constant" layer temperature. Here we summarize the relevant equations. For an individual layer, with lower and upper boundary temperatures T_L, T_U, the "linear in τ" approximation leads to the following expression for the radiance at the top of the layer (re-written from Equation 13 in (Clough et al., 1992))

$$I(\nu) = I_0(\nu)T + (1-T)\left\{B_{av}(\nu) + (B_u(\nu) - B_{av}(\nu))\left(1 - 2\left(\frac{1}{\tau} - \frac{T}{1-T}\right)\right)\right\} \tag{15}$$

where the optical depth τ includes the view angle $\tau = \tau_{layer}/cos(\theta)$ and transmission $T = exp(-\tau)$. $I_0(\nu)$ is the radiation incident at the bottom of the layer, $B_{av}(\nu)$ is the Planck radiance corresponding to the average layer temperature, while $B_u(\nu)$ is the Planck radiance corresponding to the upper boundary. For large τ, $T \to 0$ and $I(\nu) \to B_u(\nu)$. For small $\tau \to 0$ the expression can be further expanded as follows

$$I(\nu) = I_0(\nu)T + (1-T)\left\{B_{av}(\nu) + (B_u(\nu) - B_{av}(\nu))\left(\frac{\tau}{6} - \frac{\tau^3}{360} + \frac{\tau^5}{15120}\right)\right\} \quad (16)$$

Comparing to the top of layer radiance in the "constant in τ" model,

$$I(\nu) = I_0(\nu)T + (1-T)B_{av}(\nu) \quad (17)$$

one sees the expressions are identical if there is no temperature variation i.e. $(B_u(\nu) = B_{av}(\nu))$. The default kCARTA model layers are approximately 0.25 km thick (or a temperature spread of about 1.5 K for a 6K/km lapse rate) at the bottom of the atmosphere, and about 2 km thick in the stratosphere (a temperature difference of 10 K). The gaseous absorption in these upper layers is typically negligible, except deep inside the strongly absorbing 15 μm and 4 μm CO_2 bands, which is where one would expect the largest differences between a linear-in-tau versus a constant-in-tau temperature model.

7 RTA inter-comparisons : kCARTA versus LBLRTM

In this section we describe brightness temperature differences (Δ BT) between kCARTA and LBLRTM. As kCARTA is designed to be accurate for typical hyperspectral sounders, we show that after convolution the kCARTA spectral radiances compare very well against similarly convolved LBLRTM radiances; for completeness we also discuss how the monochromatic (Δ BT) change as a function of resolution in the 10-15 μm O_3 and temperature sounding regions.

For these runs we use our 49 regression profiles, with emissivity = 1 and reflectivity = 0 to exclude differences due to reflected thermal contributions. To exercise the kCARTA ray tracing, we use a ground satellite zenith angle of 24.5°which becomes a TOA satellite scan angle of 22°(typical average sounder scan angle). The tests are run at various kCARTA database resolutions. Note that when results are stated for a particular resolution, this means the kCARTA database (after 5 point boxcar integration) was at this resolution; similarly the internal LBLRTM radiances were output at a resolution such that we can apply the same 5 point boxcar for the radiance comparisons.

The comparisons are divided into two sets. For the first set of comparisons, we use an atmosphere consisting only of H_2O,CO_2,O_3, with the optical depths generated using LBLRTM v12.8. This is done to assess the linear-in-tau radiative transfer while limiting differences due to spectroscopy, especially in the high altitude 15 μm CO_2 and 10 μm O_3 sounding regions. For these tests, three resolutions spanning 605-1205 cm^{-1} were used : 0.0025 cm^{-1}, 0.0005 cm^{-1} and 0.0002 cm^{-1}.

At low resolution (0.0025 cm^{-1}), the mean differences right on top of the high altitude temperature sounding lines in the 630-700 cm^{-1} region are large ($\geq$ 10 K). However, these differences drop significantly as we increase the resolution, to within

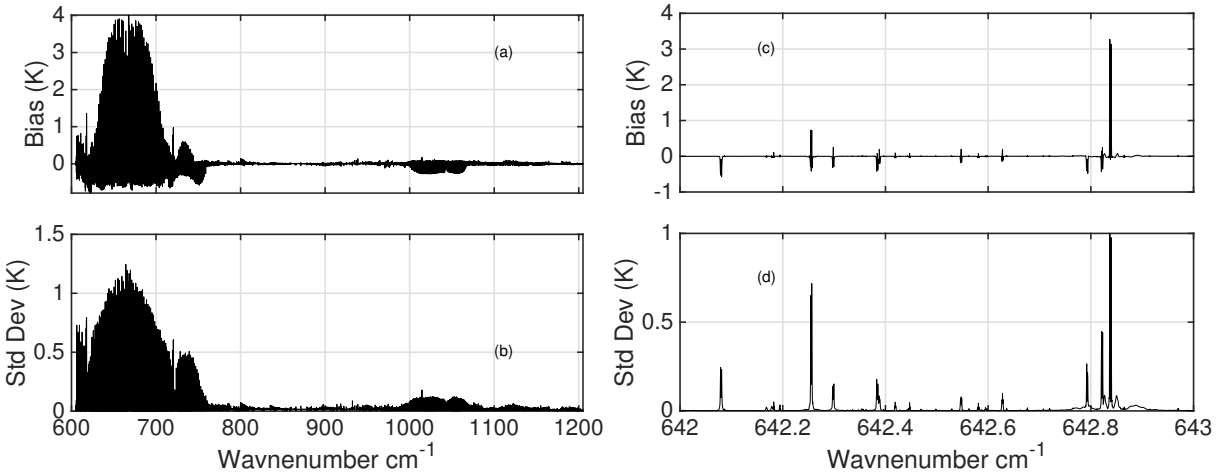

Figure 3. The top/bottom panels show the monochromatic BT differences (LBLRTM- kCARTA), with statistics obtained over 49 regression profiles, with the emissivity set to 1.0 and a 22°satellite scan angle. Both sets of panels shows the differences at 0.0005 cm^{-1} resolution when only H_2O, CO_2 and O_3 optical depths from LBLRTM v12.8 are used. The largest differences are at the peaks of the high altitude 15 um CO_2 lines, and decrease as the resolution is increased. The right hand panels are a zoom in of the left hand panels, for a typical 15 μm region.

4 K $\pm$ 1.2 K at 0.0005 cm^{-1} (default kCARTA resolution) and 1 K $\pm$ 0.4 K at 0.0002 cm^{-1}. The default kCARTA 0.0005 cm^{-1} resolution results are shown in the left hand panels (a),(b) of Figure 3. The top panel is the mean while the bottom panel is the standard deviation. Note that in the 10 μm O_3 sounding region (where the doppler broadened width of the high altitude lines would be wider than in the 15 μm region), the differences are consistently much smaller : -0.3 $\pm$ 0.1 K at 0.0005 cm^{-1} resolution, dropping to -0.1 $\pm$ 0.05 K at 0.0002 cm^{-1} resolution.

The right hand (c),(d) panels of Figure 3 are a zoom-in of a typical unit wavenumber interval deep in the 15 μm region, and shows the differences are zeros away from lines and largest around the peaks of the high sounding lines, each encompassing a very narrow spectral range of less than $\sim$ 0.005 cm^{-1}. These would be expected to contribute minimally to the convolutions using typical sounder spectral response functions, as will be shown below.

Taken together these mean that the kCARTA RTA is working as expected : in the very long wavelength 15 μm CO_2 region the differences reduce as we increase the spectral resolution while at 10 μm the differences remain quite small. We conjecture the remaining differences between kCARTA and LBLRTM are due to (a) algorithms : we use Equation 16 to fifth order while LBLRTM may use a Padé approximation and/or Equation 16 to first order; (b) there may be some very slight broadening effects right on top of the high altitude CO_2 lines that we have not captured when generating the compressed database.

For the second set of monochromatic tests, kCARTA and LBLRTM used 42 molecular gases and 13 cross section gases, using the current kCARTA default resolution of 0.0005cm^{-1}/0.0025 cm^{-1} for the spectral ranges 605-880 cm^{-1}/805-2830 cm^{-1}; the overlap region allows us to convolve the resulting radiances with AIRS Spectral Response Functions (SRFs). Note that we used the default optical depths for kCARTA (currently HITRAN 2016, except for CO_2 and CH_4 which come from LBLRTM v12.8),

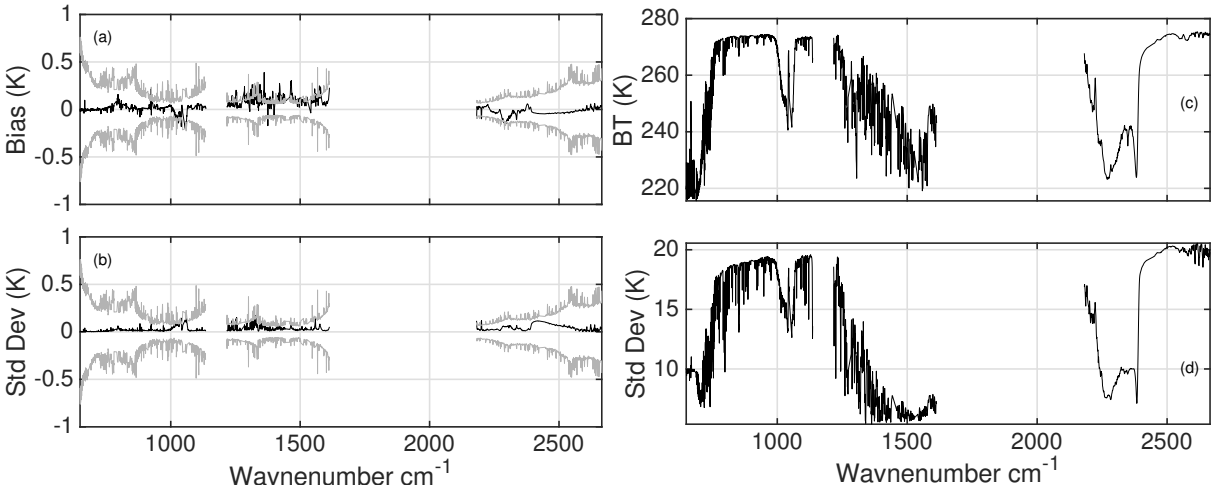

Figure 4. Results for 49 regression profiles, with 42 molecular gases and 13 cross section gases, convolved using AIRS SRFs. The emissivity was set to 1.0 and a 22° satellite scan angle. The left hand panels show the AIRS SRF convolved differences using the monochromatic differences (LBLRTM- kCARTA) seen in Figure 3, with the gray curves being the AIRS NeDT at 250 K, and are due primarily to the different spectroscopy used by the two RTAs (except for the CO_2 and CH_4 gases). The right hand panels show the mean calculated brightness temperature (top) and standard deviation (bottom). The variation in the 800-1200 cm^{-1} region (and 2400-2680 cm^{-1}) is due to surface temperature differences and column water, while the variation in the other regions such as 10 μm and 7.6 μm is due to differing gas profiles of e.g. O_3 and H_2O; the variation in the 4 μm and 15 μm regions is due to temperature profile differences.

while the LBLRTM v12.8 line-file is based on HITRAN 2012. We only briefly summarize the monochromatic differences : deep in the 15 μm they are the same as the left hand panels of Figure 3, but are noticeably different in other regions because of differences in underlying spectroscopy and (for high altitude lines) possibly also resolution; for example on top of the 10 μm O_3 lines they could be as large as 5 K. Instead we show the differences after convolution with AIRS SRFs. The left hand panels (a),(b) of Figure 4 shows the biases and standard deviations of these differences; as described the noticeable differences at 10 μm and 6.7 μm arise primarily because of spectroscopy. For completeness, the right hand panels (c),(d) show the mean BT spectra for the 49 regression panels (top panel) and the variation in computed BT (bottom panel) which are due to profile differences (temperature, H_2O and O_3) as well as surface temperatures. Any user interested in reducing the monochromatic differences could easily do so by generating and using higher resolution compressed databases.

8 Flux Computations

Longwave fluxes at the top and bottom of the atmosphere, as well as the heating and cooling rates are computed by integrating spectral radiances from Equation 2 over all angles, and over the infrared spectral region : kCARTA is limited to the spectral range 15 - 3000 cm^{-1} spanned by the different bands of kCARTA (see Appendix B). As in Section 7 the limitation of kCARTA

for flux calculations is the spectral (infrared) resolution at every layer, compared to the varying-with-height resolution employed by other models such as LBLRTM. This impacts the high altitude longwave cooling in the 15 μm CO_2 band.

We use the Rapid Radiative Transfer (Longwave) Model (RRTM-LW) (Mlawer et al., 2012) as our reference model for flux and heating rate comparisons in a clear sky atmosphere. This fast model computes fluxes and heating rates in 16 bands spanning 10 cm^{-1} to 3000 cm^{-1}, and was developed using LBLRTM; the latter uses a varying spectral resolution at each layer ($\delta\nu$ equal to 4 points per half-width in each layer) which means the spectra for the upper atmosphere layers have very high resolution. kCARTA uses the same approach as RRTM-LW and LBLRTM to compute fluxes and heating rates : the angular integration uses an exponential Gauss-Legendre with 3 or 4 terms, with a "linear in τ" layer temperature variation.

The accuracy of the flux and heating rate algorithm in kCARTA at the various resolutions was assessed by comparing fluxes and heating rates in the dominant 15 μm to 10 μm bands (fourth to eighth RRTM-LW bands, spanning 630-1180 cm^{-1}) computed using RRTM-LW and kCARTA, using the 49 regression profile set.

At 0.0025 cm^{-1} resolution the kCARTA and RRTM-LW heating rates differ by less than 0.2 K/day on average for altitudes below 40 km, but at higher altitudes the differences were much larger, and could be 1.5 K/day. Switching to the 605-1205 cm^{-1} H_2O, CO_2 and O_3 test atmosphere database at 0.0005 cm^{-1} significantly improves the results, with heating rate differences dropping to about 0.2 K/day almost everywhere.

Figure 5 shows the heating rate differences between kCARTA and RRTM-LW. The left panel shows differences between kCARTA and RRTM-LW, with the mean and standard deviation being solid and dashed respectively; the right panel shows mean calculations as a function of height. The blue curves were done at 0.0025 cm^{-1} resolution while the red curves were done at higher 0.0005 cm^{-1} resolution. While the agreement is better than 0.05 K/day in the lowest 30 km, Figure 5 shows the heating rates using the low resolution begin to differ noticeably above 45 km (blue curve); conversely the high resolution heating rates (red curves) are within 0.2 K/day till about 65 km.

9 Scattering package included with f90 kCARTA

The daily coverage of hyperspectral sounders provides us with information pertaining to the effects of cloud contamination on measured radiances. Ignoring these effects can negatively impact retrievals used for weather forecasting and climate modeling. A scattering package based on the PCLSAM (Parametrization of Cloud Longwave Scattering for use in Atmospheric Models) scheme (Chou et al., 1999) has been interfaced into f90 kCARTA (see Appendix C). The implementation allows kCARTA to compute radiances very quickly in the presence of scattering media such as clouds or aerosol. For a given scattering species and assumed particle shape and distribution, the extinction coefficients, single scattering albedo and asymmetry parameters needed by the scattering code are stored in tables as a function of wavenumber and effective particle size (for a particle amount of 1 g/m^2). The PCLSAM packge is optimized for use in the thermal infared, away from regions where solar contributions are important. As kCARTA currently does not handle e.g. Rayleigh scattering, one can easily use kCARTA to output monochromatic optical depths that can be imported into well known scattering packages. More details about PCLSAM and our cloud representation models are found in Appendix C.

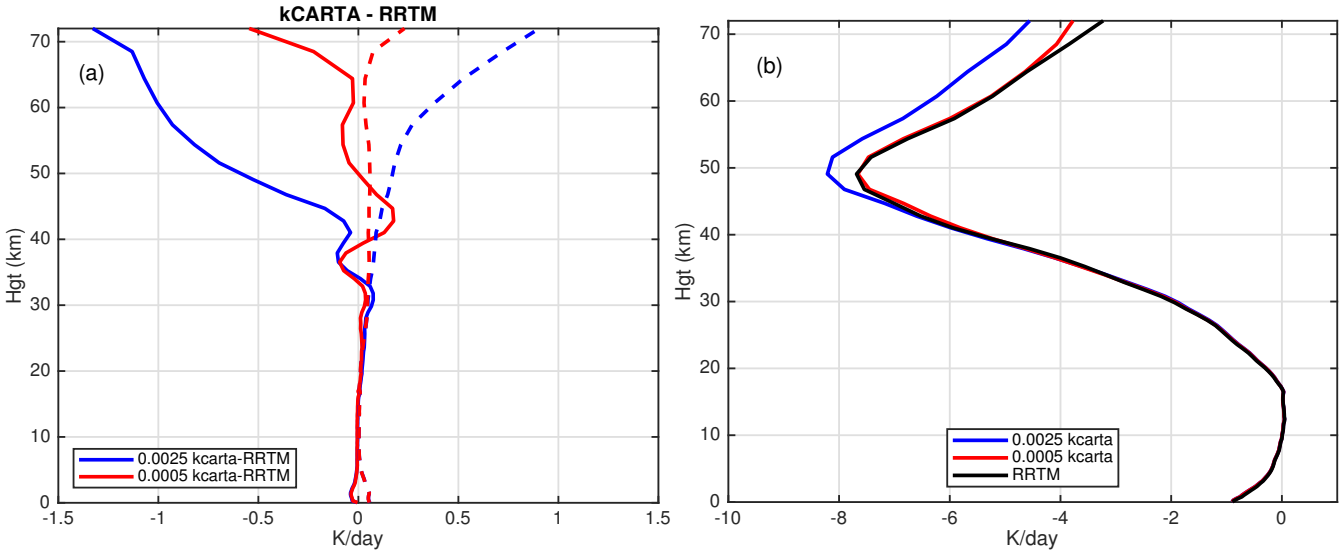

Figure 5. Heating rates for the 630-1180 cm^{-1} region computed using low (0.0025 cm^{-1}; blue curves) and high (0.0005 cm^{-1}; red curves) resolution kCARTA databases for 49 spanning Earth atmosphere profiles, compared to RRTM-LW. (a) The left panel shows differences in the heating rates, while (b) the right panel shows the mean heating rates.

10 Conclusions

We have described the details of a very fast and accurate pseudo- monochromatic code, optimized for the thermal infrared spectral region used by operational weather sounders for thermodynamic retrievals. It is much faster than line-by-line codes, and the accuracy of its spectroscopic database has been extensively compared against GENLN2 and more recently to LBLRTM. Updating the spectroscopy in a selected wavenumber region for a specified gas is as simple as updating the relevant file(s) in the database : for example, our custom UMBC-LBL enables us to re-build entire databases within weeks of the latest HITRAN release.

The computed clear sky radiances includes a fast, accurate estimate of the background thermal radiation. Analytic temperature and gas amount jacobians can be rapidly computed. Early in the AIRS mission, comparisons of AIRS observations against kCARTA simulations allowed for the quick implementation of modifications to gas optical depths : our modifications to the CKD2.4 and MT-CKD 1.0 continuum versions are very similar to what is now in the MT-CKD2.5 version. We now use the MT-CKD 3.2 continuum, together with the N_2 and O_2 continuum contributions bundled with that same version. We use two resolutions in the infrared : 0.0005 cm^{-1} for the 605-880 cm^{-1} region (to accurately resolve the high altitude CO_2 lines) and 0.0025 cm^{-1} elsewhere; an user can easily switch to an alternate resolution by generating the appropriate compressed databases for use with kCARTA, though this could be at the expense of speed (at these current resolutions kCARTA takes 30 seconds to compute TOA spectra from 605-2830 cm^{-1} while LBLRTM takes over three minutes). Tests show that brightness temperature differences between kCARTA and for example LBLRTM are largest right on top of a small number of high altitude

temperature sounding lines in the 15 μm region (and close to zero elsewhere); these differences reduce as the resolution is increased. Since the disparity is right at the peaks of the lines, the differences after convolution with a typical sounder SRF such as AIRS are on average much smaller than the NeDT.

kCARTA is fast enough to be used in Optimal Estimation retrievals for instruments spanning a reasonably small wavenumber range. The kCARTA database has been extended to include 15-44000 cm^{-1}, which eventually needs to be updated to HITRAN 2016 (see the Appendix). In the future we plan to augment the optical depth calculations performed by UMBC-LBL by using speed-dependent lineshapes as parameters become available.

Appendix A: Code availability

The UMBC-LBL code has been developed in Matlab, with extensive use of Mex files to speed up loops. The package is available at https://github.com/ sergio66/UMBC_LBL, and is fully described in (De Souza-Machado et al., 2002). The compression code is available upon request.

The f90 and Matlab versions of kCARTA can be cloned from https://github.com/ sergio66/kcarta_gen and https://github.com/strow/kcarta-matlab respectively.

A1 UMBC-LBL and kCARTA downloads and auxiliary requirements

The kCompressed Database is supplied in Fortran little-endian binary files that contain the optical depths for a specific gas. Each file contains optical depths at 10000 spectral points $\times$ average pressures corresponding to the 100 AIRS layers. Links to the (605 - 2830 cm^{-1}) compressed database can be found at http://asl.umbc.edu/pub/packages/kCompressedDatabase.html

We also supply the US Standard Profile for all gases in the database, and kLAYERS, a program that takes in a point profile (from sondes and NWPs) and outputs an AIRS 100 layer path averaged profile (in molecules/cm^2). kLAYERS needs our supplied HDF file implementation (RTP) source code.

The Matlab version should work with R2012+ while the compiler for the Fortran version must support structures, such as Absoft, ifort and PGF. As the RTP file contains the atmospheric profile and scan geometry, both the Matlab and f90 kCARTA only need a simple additional (namelist) file to drive either code. The f90 version of kCARTA outputs binary files, which typically have header information such as kCARTA version number, number of layers and gases and parameter setting values, followed by panels, each 10000 points long, containing the optical depths, radiances, jacobians or fluxes computed and output by kCARTA. A number of Matlab based readers can then be used to further process the kCARTA output as needed. More information is found at http://asl.umbc.edu/pub/packages/ kcarta.html.

A new compressed database (spanning the infrared 500-2830 cm^{-1} region) is generated for kCARTA every four years, roughly within a few months of a HITRAN database release. The current f90 version described in this paper is identified on github as SRCv1.21_f90 and currently uses HITRAN 2016 line parameters for all gases except CO_2 and CH_4 where we used LBLRTM v12.8 optical depths, together with MT-CKD3.2 continuum. These were used to generate the most recent

SARTA v2.01 fast model coefficients; earlier SARTA versions were developed using kCARTA v1.07 and v1.18 (with HITRAN databases updated as they became available).

Appendix B: Available spectral regions and f90 kCARTA features

Table B1. Spectral bands for kCARTA

Band (cm^{-1})	Point Spacing (cm^{-1})	Band center (μm)	number of files
15-30	0.00005	444.4	30
30-50	0.00010	250.0	20
50-80	0.00015	153.8	20
80-140	0.00025	90.9	28
140-300	0.00050	45.4	34
300-500	0.00100	25.0	21
500-605	0.00050	18.1	21
605-880*	0.00050	14.18	40
805-2830*	0.00250	5.5	81
2830-3550	0.00250	3.1	30
3550-5550	0.00100	2.2	21
5550-8250	0.01500	1.4	19
8250-12000	0.02500	0.98	16
12000-25000	0.05000	0.54	26
25000-44000	0.10000	0.29	19

The UMBC-LBL line-by-line code has been used to generate optical depths in the spectral regions seen in Table B1. The 605-2830 cm^{-1} band is marked with an asterisk, since our work focuses on this spectral region. The current database in this spectral region uses lineshape parameters from HITRAN 2016. The Van Vleck and Huber lineshape is used for all HITRAN molecules from ozone onward; water vapor uses the "without basement" plus MT-CKD 3.2, and CO_2,CH_4 use line-mixing optical depths generated from LBLRTM v12.8. Note that in the important 4.3 μm temperature sounding region, the f90 version can also include the N_2/H_2O and N_2/CO_2 Collision Induced Absorption (CIA) effects modeled in (Hartmann et al., 2018; Tran et al., 2018), which depend on CO_2,H_2O and N_2 absorber amounts.

A clear-sky radiance calculation in the infrared takes about 30 seconds, using a 2.8 GHz 32 core multi-threading Intel machine. The run-time goes to 120 seconds if jacobians are also computed (for 9 gases). A full radiance calculation from 15 to 44000 cm^{-1} takes less than 5 minutes.

Table B2 lists a number of the features of kCARTA, with the ones marked by a asterisk only available in the f90 version. Note that the tables defaults to describing the spectroscopy for the infrared region.

Table B2: kCARTA features; * indicates currently only available in the f90 version

Feature	Default	Options
SPECTROSCOPY		
(1) IR Database	HITRAN 2016	HITRAN 2012, GEISA 2015
(2) Resolution	0.0005/0.0025 cm^{-1}	can make other resolutions
(3) Molecular gases	HITRAN ID 1-42	choose some
(4) Cross-section gases	HITRAN (CFCs etc)	choose some
(5) Water continuum	MT-CKD 3.2	e.g. MT-CKD 1.0, 2.5
(6) CO_2 line mixing	from LBLRTM v12.8	UMBC-LBL line mixing
(7) CO_2/H_2O, CO_2/N_2 CIA*	off	Hartmann and Tran*
(8) CH_4 line mixing	from LBLRTM v12.8	None (voigt)
(9) O_2 and N_2	HITRAN 2016 and LBLRTM v1.28 continuum	
(10) NLTE	line by line *	SARTA approximation
(11) Uncompressiom	linear	spline
RADIATIVE TRANSFER	CLEAR SKY	
(1)Temperature variation	Linear in τ*	Constant
(2) Background thermal	acos(3/5) in upper layers, accurate angle lower layers	acos(3/5) all layers gauss quadrature*
(3) Background thermal Surface reflection	lambertian $(1-\epsilon_s(\nu))/\pi$	
(4) Solar reflection	user specified	
(5) Ray tracing	Spherical atmosphere,n=1	n varies*
(6) Direction	upwelling	downwelling
(7) Solar	from tables	use 5600 K
(8) Jacobians	100 layer T, WV, weighting functions acos(3/5) backgrnd thermal	column jacs
(9) Fluxes*	upwell, downwell	Heating rates
RADIATIVE TRANSFER	ALL SKY	
(1) TwoSlab Cloud model*	PCLSAM	fluxes and jacobians
(2) couple to LBLDIS*		

The spline versus linear temperature interpolation differences, as tested on 49 regression profiles, are 0.0004 $\pm$ 0.0040 K, with a maximum absolute difference of 0.342 K (in the 15 um region).

Appendix C: PCLSAM scattering algorithm

The PCLSAM scattering algorithm for longwave radiances has applications ranging from dust retrievals (De Souza-Machado et al., 2010), to modeling the effects of clouds on sounder data (Matricardi, 2005; Vidot et al., 2015). This scattering model changes the extinction optical depth from $k(\nu)$ to a parametrized number $k^{scatterer}_{eff.extinction}(\nu)$ (Chou et al., 1999), and is designed for cases of the single scattering albedo ω being much less than 1, such as in the thermal infrared, where ω for cirrus and water droplets and aerosols is typically on the order of 0.5.

Since $k^{scatterer}_{eff.extinction}(\nu)$ is now effectively the absorption due to the cloud or aerosol, for each layer i that contains scatterers we replace the gas absorption optical depth with the total absorption optical depth

$$k_{total}(\nu) = k^{gases}_{atm}(\nu) + k^{scatterer}_{eff.extinction}(\nu) \tag{C1}$$

where(Chou et al., 1999) $k^{scatterer}_{eff.extinction}(\nu) = k^{scatterer}_{extinction}(\nu) \times (1-\omega(\nu))(1-b(\nu))$ and the backscatter $b(\nu) = (1-g(\nu))/2$, with $g(\nu)$ being the asymmetry factor. Using this for every layer containing scatterers, the radiative transfer algorithm is now the same as clear sky radiative transfer, with very little speed penalty.

kCARTA is capable of using a TwoSlab (De Souza-Machado et al., 2018) cloud representation scheme for use with PCLSAM. This allows for non unity fractions for up to two clouds, so that radiative transfer then assumes the total radiance is a sum of four radiance streams (clear, cloud 1, cloud 2 and the cloud overlap) weighted appropriately :

$$r(\nu) \quad = \quad c_{overlap} r^{(12)}(\nu) + c_1 r^{(1)}(\nu) + c_2 r^{(2)}(\nu) + f_{clr} r^{clr}(\nu) \tag{C2}$$

With this model kCARTA allows the user to specify up to two types of scatterers in the atmosphere (ice/water, ice/dust, water/dust or even ice/ice, water/water, dust/dust); the two scatterers are placed in separate "slabs" which occupy complete AIRS layers and are specified by cloud top/bottom pressure (in millibars), cloud amount (in g/m2), cloud effective particle diameter (in μm). After the computations are done, all five radiances are output when two clouds are defined (overlap, two clouds separately, clear, and the weighted sum), and three radiances if only one cloud is defined (one cloud, clear, weighted sum).

Analytic jacobians for temperature, gas amounts, and cloud micro-physical parameters (effective size and loading) can also be computed, as can be fluxes and associated heating rates, though the slab boundaries could introduce spikes in the heating rate profiles.

kCARTA does not have built-in multiple scattering capabilities to handle for example Rayleigh scattering in the ultra-violet. To handle this we have written Matlab routines to read in kCARTA optical depths and pipe them into LBLDIS (Turner et al., 2003; Turner, 2005), a code that merges optical depths and scattering using the extensively tested Discrete Ordinates Radiative Transfer (DISORT) (Stamnes et al., 1988) algorithm.

Author contribution

Sergio DeSouza-Machado prepared the manuscript with contributions from all (living) co-authors. The initial compressed database coding and testing was done by L. Strow, H. Motteler and S. Hannon. Following this deS-M wrote the Fortan and Matlab wrapper codes for clear sky radiative transfer and jacobians, which were tested and validated by the other authors. Scattering and flux capabilities were added and tested by deS-M.

Competing interests

The authors declare that they have no conflict of interest.

Acknowledgments

We thank the anonymous reviewers whose comments/suggestions helped improve this manuscript. This work was supported in part by NASA grant number NNG04GG03G-2. Dave Tobin of UW-Madison helped with UMBC-LBL CO_2 line-mixing code and modifying the water continuum coefficients. Dave Edwards of NCAR provided the GENLN2 line-by-line code to compare kCARTA against. Both Dave Edwards and Manuel Lopez-Puertas of the Instituto de Astrofisica de Andalucia (Spain) contributed to the NLTE portions of the code. Optical depth and flux comparisons against LBLRTM were facilitated by Eli Mlawer (Atmospheric and Environmental Research, Lexington MA), while Guido Masiello (University of Basilicata, Italy) helped with the radiance inter-comparisons.

References

Aumann, H., Chahine, M., Gautier, C., Goldberg, M., Kalnay, E., McMillin, L., Revercomb, H., Rosenkranz, P., Smith, W., Staelin, D., Strow, L., and Susskind, J.: AIRS/AMSU/HSB on the Aqua Mission: Design, Science Objectives, Data Products and Processing Systems, IEEE Trans. Geosci. Remote Sens., 41, 253–264, 2003.

Buehler, S., Eriksson, P., and Lemke, O.: Absorption lookup tables in the radiative transfer model ARTS, J. Quant. Spectrosc. Rad. Trans., 112, 1559–1567; doi:10.1016/j.jqsrt.2011.03.008, 2011.

Chou, M.-D., Lee, K.-T., Tsay, S.-C., and Fu, Q.: Parameterization for Cloud Longwave Scattering for use in Atmospheric Models, J. Climate, 12, 159–169, 1999.

Clerbaux, C., Boynard, A., Clarisse, L., George, M., Hadji-Lazarro, J., Herbin, H., Hurtmans, D. Pommier, M., Razavi, A., Turquety, S., Wespes, C., and Coheur, P.-F.: Monitoring of atmospheric composition using the thermal infrared IASI/MetOp sounder, Atmos. Chem. and Phys., 9, 6041–6054, doi:10.5194/acp–9–6041–2009, 2009.

Clough, S. and Iacono, M. J.: Line by line calculation of atmospheric fluxes and cooling rates.2. Application to Carbon-Dioxide,Ozone , Methane, Nitrous-Oxide and the Halocarbons, J. Geophys. Res. A, 100, D8, 16 519–16 535, 1995.

Clough, S., Kneizys, F., Davies, R., Gamache, R., and Tipping, R.: Theoretical line shape for H_2O vapour; Application to the continuum, in: Atmospheric water vapour, edited by Deepak, A., Wilkerson, T., and Rhunke, L., pp. 25–46, Academic Press, NY, 1980.

Clough, S., Shephard, M., Mlawer, E., Delamere, J., Iacono, M. J., Cady-Pereira, K., Boukabara, S., and Brown, P.: Atmospheric radiative transfer modeling : a summary of the AER codes, J. Quant. Spectrosc. Rad. Trans., 91, 233–244doi:10.016/j.qsrt2004.05.058, 2005.

Clough, S. A., Kneizys, F. X., and Davies, R. W.: Line Shape and the Water Vapor Continuum, Atmos. Res., 23, 229–241, 1989.

Clough, S. A., Iacono, M. J., and Moncet, J. L.: Line-by-line calculations of atmospheric fluxes and cooling rates: application to water vapor, J.Geophys.Res., 97, 15,761–15,785, 1992.

De Souza-Machado, S., Strow, L. L., Tobin, D., Motteler, H., and Hannon, S.: UMBC-LBL: An Algorithm to Compute Line-by-Line Spectra, Tech. rep., University of Maryland Baltimore County, Department of Physics, http://asl.umbc.edu/rta/lbl.html, 2002.

De Souza-Machado, S., Strow, L. L., Motteler, H., Hannon, S., Lopez-Puertas, M., Funke, B., and Edwards, D.: Fast Forward Radiative Transfer Modeling of 4.3 um Non-Local Thermodynamic Equilibrium effects for the Aqua/AIRS Infrared Temperature Sounder, Geophys. Res. Lett., 34, doi:10.1029/2006GL026 684,L01 802, 2007.

De Souza-Machado, S., Strow, L. L., Imbiriba, B., McCann, K., Hoff, R., Hannon, S., Martins, J., Tanré, D., Deuzé, J., Ducos, F., and Torres, O.: Infrared retrievals of dust using AIRS: comparisons of optical depths and heights derived for a North African dust storm to other collocated EOS A-Train and surface observations, J. Geophys. Res., 115, doi:10.1029/2009JD012 842,D15 201, 2010.

De Souza-Machado, S., Strow, L. L., Tangborn, A., Huang, X., Chen, X., Liu, X., Wu, X., and Yang, Q.: Single-footprint retrievals for AIRS using a fast TwoSlab cloud-representation model and the SARTA all-sky infrared radiative transfer algorithm, Atmos. Meas. Tech., 11, 529–550,https://doi.org/10.5194/amt–11–529–2018, 2018.

Dudhia, A.: The Reference Forward Model (RFM), J. Quant. Spectrosc. Rad. Trans., 186, 243–253, 2017.

Edwards, D.: GENLN2: A General Line–by–Line Atmospheric Transmittance and Radiance Model, *NCAR Technical Note 367+STR*, National Center for Atmospheric Research, Boulder, Colo., 1992.

Edwards, D. P., Lopez-Puertas, M., and López-Valverde, M.: Non LTE Studies of 15 um bands of CO2 for Atmospheric Remote Sensing, J.Geophys.Res., 98, 14 955–14 977, 1993.

Edwards, D. P., Lopez-Puertas, M., and Gamache, R.: The Non LTE COrrection to the Vibrational Component of the Internal Partition Sum for Atmospheric Calculations, J. Quant. Spectrosc. Rad. Trans., 59, 423–436, 1998.

Farmer, C. B. and Norton, R.: Atlas of the Infrared Spectrum of the Sun and the Earth Atmosphere from Space. Volume I, The Sun, NASA JPL publication 1224, NASA, Pasadena, CA, 1989.

Farmer, C. B., Raper, O., and O'Callaghan, F.: Final report on the first flight of the ATMOS instrument during the Spacelab 3 mission, April 29 through May 6, 1985, JPL publication **87–32**, Jet Propulsion Laboratory, Pasadena, CA, 1987.

Gambacorta, A.: The NOAA Unique CrIS/ATMS Processing System (NUCAPS): Algorithm Theoretical Basis Documentation, Tech. rep., NCWCP, http://www.ospo.noaa.gov/Products/atmosphere/soundings/nucaps/docs/NUCAPS_ATBD_20130821.pdf, 2013.

Goody, R. and Yung, Y.: Atmospheric Radiation: Theoretical Basis, Oxford University Press, 1989.

Gordon, I., Rothman, L., Hill, C., Kochanov, R., and Tan, Y. e. a.: The HITRAN 2016 molecular spectroscopic database, J. Quant. Spectrosc. Rad. Trans., 203, 3–69,https://doi.org/10.1016/j.jqsrt.2017.06.038, 2017.

Han, Y., Revercomb., H., Cromp, M., Strow, L., Chen, Y., and Tobin, D.: Suomi NPP CrIS measurements, sensor data record algorithm, calibration and validation activities, and record data quality, J. Geophys. Res., 118, doi:10.1002/2013JD020 344, 2013.

Hartmann, J.-M., Boulet, C., Tran, D., Tran, H., and Baranov, Y.: Effect of humidity on the absorption continua of CO2 and N2 near 4 um : calculations, comparisons with measurements, consequences on atmospheric spectra, J. Chem. Phys, 148, 54 304, 2018.

Hoffman, L. and Alexander, M.: Retrieval of stratospheric temperatures from Atmospheric Infrared Sounder radiance measurements for gravity wave studies, J. Geophys. Res., 114, D07 105;doi:10.1029/2008JD011 241, 2009.

Husson, N., Armante, R., Scott, N., Chedin, A., Crepeau, L., Boitammine, C., Bouhdaoui, A., Crevoisier, C., Capelle, V., Boone, C., Poulet-Croviser, N., Barbe, A., Benner, C., Boudon, V., Brown, L., Buldyreva, J., Campargue, A., L.H., C., Makie, A., and et. al.: The 2015 edition of the GEISA spectroscopic database, J. Mol. Spectr., 327, 31–72; https://doi.org/10.1016/j.jms.2016.06.007, 2015.

Lamouroux, J., Tran, H., Laraia, A. L., Gamache, R. R., Rothman, L. S., Gordon, I. E., and Hartmann, J.-M.: Updated database plus software for line-mixing in CO2 infrared spectra and their test using laboratory spectra in the 1.5-2.3 um region, J. Quant. Spectrosc. Rad. Trans., 111, 2321–2331,10.1016/j.jqsrt.2010.03.006, 2010.

Lamouroux, J., Rogalia, L., Thomas, X., Vander Auwera, J., Gamache, R., and Hartmann, J.-M.: CO2 line-mixing database and software update and its tests in the 2.1 um and 4.3 um regions, J. Quant. Spectrosc. Rad. Trans., 151, 88–96; https://doi.org/10.1016/j.jqsrt.2014.09.017, 2015.

Liou, K.: An Introduction to Atmospheric Radiation, Academic Press, 1980.

Liu, X., Smith, W., Zhou, D., and Larar, A.: Principal component based radiative transfer model for hyperspectral sensors : theoretical concepts, Appl. Opt, 45, 201–209, 2006.

Lopez-Puertas, M. and Taylor, F.: NONLTE Radiative Transfer in the Atmosphere, World Scientific Publishing, 2001.

Matricardi, M.: The inclusion of aerosols and clouds in RTIASI, the ECMWF fast radiative transfer model for the infrared atmospheric sounding interferometer, 2005.

Mlawer, E. J., Payne, V. H., Moncet, J.-L., Delamere, J., Alvarado, M., and Tobin, D.: Development and recent evaluation of the MT_CKD model of continuum absorption, Phil. Trans. Roy. Soc. A, 370, 1–37, doi:10.1098:rsta.2011.0295, 2012.

Nalli, N., Smith, W., and Liu, Q.: Angular Effect of Undetected CLouds in Infrared Window Radiance Observations : Aircraft Experimental Analysis, J.Atmos.Sci., 73, 1987–2011,DOI: 10.1175/JAS–D–15–0262.1, 2016.

Niro, F., Jucks, K. W., and Hartmann, J. M.: Spectra calculations in central and wing regions of CO2 IR bands between 10 and 20 um : Software and database for the computation of atmospheric spectra, J. Quant. Spectrosc. Rad. Trans., 95, 469–481, 2005.

Rodgers, C.: Inverse Methods for Atmospheric Sounding, World Scientific, Singapore, 2000.

Rothman, L. S., Gordon, I., Babikov, Y., Barbe, A., Benner, D., and Bernath, P. e. a.: The HITRAN 2012 molecular spectroscopic database, J. Quant. Spectrosc. Rad. Trans., 130, 4–50, 2013.

Saunders, R., Matricardi, M., and Brunel, P.: An improved fast radiative transfer model for the assimilation of satellite radiance observations, Quart.J.Roy.Meteorol.Soc., 125, 1407–1425, 1999.

Schreier, F., Garcia, S., Hedelt, P., Hess, M., Mendrok, J., Vasquez, M., and Xu, J.: GARLIC — A general purpose atmospheric radiative transfer line-by-line infrared-microwave code: Implementation and evaluation, J. Quant. Spectrosc. Rad. Trans., 137, 29–50, 2014.

Stamnes, K., Tsay, S.-C., Wiscombe, W., and Jayaweera, K.: Numerically Stable Algorithm for discrete ordinate method Radiative Transfer in multiple scattering and emitting layered media, Appl. Opt, 27, 2502–2509, 1988.

Strow, L., Motteler, H., Benson, R., Hannon, S., and De Souza-Machado, S.: Fast Computation of Monochromatic Infrared Atmospheric Transmittances using Compressed Look-Up Tables, J. Quant. Spectrosc. Rad. Trans., 59, 481–493, 1998.

Strow, L., Hannon, S., DeSouza-Machado, S., Tobin, D., and Motteler, H.: An Overview of the AIRS Radiative Transfer Model, IEEE Transactions on Geosciences and Remote Sensing, 41, 303–313, 2003.

Strow, L. L. and Pine, A. S.: Q-branch line mixing in N_2O: Effects of ℓ-type doubling, J. Chem. Phys., 89, 1427, 1988.

Susskind, J., Barnet, C., and Blaisdell, J.: Atmospheric and Surface Parameters from Simulated AIRS/AMSU/HSB Sounding Data: Retrieval and Cloud Clearing Methodology, Adv. Space. Sci, 21, 369–384 doi:10.1016/S0273–1177(97)00 916–2, 1998.

Tjemkes, S., Patterson, T., Rizzi, R., Shephard, M., Clough, S., Matricardi, M., Haigh, J., Hopfner, M., Payan, S., Trotsenko, A., Scott, N., Rayer, P., Taylor, J., CLerbaux, C., Strow, L., DeSouza-Machado, S., Tobin, D., and Knuteson, R.: The ISSWG Line-by-line Intercomparison Experiment, J. Quant. Spectrosc. Rad. Trans., 77, 433, 2002.

Tobin, D. C., Strow, L. L., Lafferty, W. J., and Olson, W. B.: Experimental Investigation of the Self- and N_2- Broadened Continuum within the ν_2 Band of Water Vapor, Appl. Opt., 35, 1, 1996.

Tran, H., Flaud, P.-M., Gabard, T., Hase, F., Von Clarmann, T., Camy-Peyret, C., Payan, S., and Hartmann, J.-H.: Model, Software and database for line-mixing effects in the v3 and v4 bands of CH4 and tests using laboratory and planetary measurements. I. N2 (and air) broadening and the Earth atmosphere, J. Quant. Spectrosc. Rad. Trans., 101, 284–305, 2006.

Tran, H., Turbet, M., Chelin, P., and Landsheere, X.: Measurements and modeling of absorption by CO2+H2O mixtures in the spectral region beyond the CO2 v3 bandhead, Icarus, 306, 116–121, 2018.

Turner, D.: Arctic mixed-phase cloud properties from AERI-lidar observations: Algorithm and results from SHEBA, J.Appl. Met, 44, 427–444, 2005.

Turner, D., Ackerman, S., Baum, B., Revercomb, H., and Yang, P.: Cloud Phase Determination using ground based AERI observations at SHEBA, J.Appl. Met, 42, 701–715, 2003.

Van Vleck, J. H. and Huber, D. L.: Absorption, emission, and linebreadths: A semihistorical perspective, Rev. Mod. Phys., 49, 939, 1977.

Vidot, J., Baran, A., and Brunel, P.: A new ice cloud parameterization for infrared radiative transfer simulation of cloudy radiances: Evaluation and optimization with IIR observations and ice cloud profile retrieval products, J. Geophys. Res., 120, doi:10.1002/ 2015JD023 462,6937–6951, 2015.

Vincent, R. and Dudhia, A.: Fast radiative transfer using monochromatic look-up tables, J. Quant. Spectrosc. Rad. Trans., 186, 254–264,https://doi.org/10.1016/j.jqsrt.2016.04.011, 2017.

Zorn, S., von Clarmann, T., Echle, G., Funke, B., Hase, F., Hopfner, M., Kemnitzer, H., Kuntz, M., and Stiller, G.: KOPRA: Analytic expressions for modelling radiative transfer and instrumental effects, Tech. rep., Karlsruhe University, Germany, https://www.imk-asf.kit.edu/downloads/SAT/kopra_docu_part02.pdf, 2002.